Summer Surface Albedo of Sea Ice in Pacific Arctic Sector as Measured during the CHINARE 2010 cruise

Authors: Xia, Wentao, Xie, Hongjie, Ke, Changqing, Zhao, Jinping, Lei, Ruibo, et al.

Source: Arctic, Antarctic, and Alpine Research, 47(4) : 645-656

Published By: Institute of Arctic and Alpine Research (INSTAAR), University of Colorado

URL: https://doi.org/10.1657/AAAR0014-090

Arctic, Antarctic, and Alpine Research, Vol. 47, No. 4, 2015, pp. 645–656

Summer surface albedo of sea ice in Pacific Arctic sector as measured during the CHINARE 2010 cruise

Wentao Xia[1]
Hongjie Xie[1,5]
Changqing Ke[2]
Jinping Zhao[3]
Ruibo Lei[4] *and*
Stephen F. Ackley[1]

[1]Laboratory for Remote Sensing and Geoinformatics, University of Texas at San Antonio, One UTSA Circle, San Antonio, Texas 78249, U.S.A.
[2]School of Geographic & Oceanographic Sciences, Nanjing University, 163 Xianlin Avenue, Qixia district, Nanjing 210023, China
[3]College of Physical and Environmental Oceanography, Ocean University of China, 238 Songling Street, Qindao 266100, China
[4]Key Laboratory for Polar Science of the State Oceanic Administration, Polar Research Institute of China, 451 Jinqiao Street, Pudong new district, Shanghai 200136, China
[5]Corresponding author: Hongjie.xie@utsa.edu

DOI: http://dx.doi.org/10.1657/AAAR0014-090

Abstract

Knowledge of Arctic snow and ice surface albedo is essential to understand local energy budget and snow/ice albedo feedback under global warming scenario. In situ measured albedo plays an essential role by providing ground truth reference for remote sensing monitoring of albedo at large scale. Such measurements with portable and fixed-location spectroradiometers were conducted in one 12-day (long-term) and several short-term (3–4 hours) ice stations over the Pacific Arctic sector during the summer 2010 Chinese National Arctic Research Expedition (CHINARE). Results show that the wavelength-integrated albedo across 350 to 2200 nm of bare ice was ~0.56 to 0.68 in the lower latitudes and marginal ice zone, while albedo of snow-covered ice reduced from 0.75–0.86 to 0.42–0.61 during the mid-August period of the 12-day ice station (86°48′N to 87°20′N). The albedo variation and evolution of melt ponds were examined with details during the 12-day ice station. It is found that albedo of melt pond reduced from 0.68 (melt pond snow, 9 August) and 0.66 (melt pond ice, 9 August) to 0.32 (melt pond water and ice, 17 August) in one week as a rainfall event occurred. Such rapid decreasing of snow and sea ice albedo and evident difference between the pack ice zone and marginal ice zone may contribute to the surface albedo feedback and rapidly shrinking summer sea ice extent in the Arctic Ocean.

Introduction

The surface albedo is defined as the ratio of solar energy reflected upward over energy incident upon the same surface (Hanesiak et al., 2001). The homogeneous high-albedo snow-covered sea ice in Arctic late winter to early spring maintains the regional low-energy status, governing local heat budget by reflecting incident solar energy and preventing heat transfer from the warmer ocean to the atmosphere. In Arctic summer, snow-covered sea ice melts and turns into a heterogeneous combination of wet snow, bare ice, melt ponds, leads, and open water (Perovich et al., 2002). This melting process significantly lowers the surface albedo of Arctic sea ice, amplifies the absorption of the incident solar radiation, and triggers the well-defined ice-albedo feedback (Perovich et al., 2002). This positive feedback is further enhanced under current global warming context, as the lateral and surface melting become more severe in summer (Perovich et al., 2011; Curry et al., 1995; Stroeve et al., 2011).

Monitoring sea ice (and its snow surface) albedo is the foundation in the understanding and modeling of Arctic climatic and hydrologic processes, and the prediction of the future trend of ice cover changes (Lindsay and Rothrock, 1994; Morassutti and Ledrew, 1996; Hanesiak et al., 2001; Perovich et al., 2002). In situ observations of surface albedo directly provide the ground truth information required in validation and calibration of remote sensing applications, and the parameterization in climate models (Barry, 1996; Gardner and Sharp, 2010; Pedersen and Winther, 2005; Robinson et al., 1992). These field-based radiometric measurements of sea ice optical properties (like reflectance, scattering, and transmittance) are also essential in analyzing regional energy budget and albedo feedback (Ebert and Curry, 1993; Moritz and Perovich, 1996; Bitz et al., 2001; Holland et al., 2006).

There has been extensive field work addressing these ice surface changes. The albedo measurements conducted in the Surface Heat Budget of the Arctic Ocean (SHEBA) field experiment (1997–1998) (Perovich et al., 2002) examined the seasonal evolution of sea ice albedo on multi-year sea ice in the Beaufort Sea. According to SHEBA observations in the summer, the albedo (integrated through 300–3000 nm wavelength) of melting snow over multi-year ice was 0.6–0.7, and the melt pond albedo was 0.4 (light ponds) and 0.2 (dark ponds). The field measurements near Barrow, Alaska (Grenfell and Perovich, 2004; Perovich and Polashenski, 2012) investigated the inter-annual surface albedo changes of seasonal sea ice and found a more rapid summer surface albedo decrease than that observed in the Beaufort Sea during SHEBA, from 0.85 (cold snow) to 0.6 (melting snow) in 7 days, and then a further decrease to 0.32 (pond formation) in next 7 days. The ground and airborne surface albedos measured in Wellington Channel, Canadian Archipelago, were compared with satellite imagery, to address regional albedo changes through upscaling (Hanesiak et al., 2001). They showed the combined regional estimation of the surface albedo of 0.55 to 0.57, based on measured albedos of wet snow (0.67), thin wet and saturated snow (0.52–0.65), and light melt pond (0.32–0.36).

1523-0430/04 $7.00

In the 2010 Chinese National Arctic Research Expedition (CHINARE, 2010), field observations on various surface objects were conducted on the Pacific sector of the Arctic, from July 27 to August 24 (Xie et al., 2013). The field work includes measurements of surface albedo of snow cover, snow-covered ice, and melt ponds across different areas of the Pacific Arctic sector, providing an opportunity to examine the changing albedo across distinct areas during a rapidly changing summer.

Method

INSTRUMENTATIONS

The expedition entered the sea ice zone on 20 July 2010 and exited there on 28 August 2010. An Analytical Spectral Devices (ASD) Field Spec 3 portable spectroradiometer was used for albedo measurements at seven of the eight short-term (2–4 hours each) and one 12-day (long-term) ice stations (Fig.1, Table 1). There was no radiometric measurement in the second short-term ice station (IS-2) due to expedition schedule. A 180-degree field of view (FOV) sensor (i.e., cosine sensor) was used to measure spectral irradiance at 350–2500 nm spectra, with spectral resolution of 1–2 nm. For the sixth and eighth short-term ice stations, only the radiance measurements with 25-degree and 5-degree FOV sensors were conducted, and therefore surface albedo is not calculated for the two stations. The sensor was attached to the end of a pole (1 m in length) and was handheld to a position where the sensor was right above the surface objects. The incident solar irradiation was measured by upward-looking measurement to the sky. Objects measured include the regular snow cover, bare ice, sea ice (specifically refers to the bare ice exposed at the bottom of snow pits for this paper), snow cover on melt pond ice, ice on melt pond water, and water in melt pond.

In addition to the ASD spectroradiometer, a CMA6 albedometer (Kipp & Zonen Co., Netherlands) (wavelength range at 285–2800 nm) was used only during the 12-day ice station period. The CMA6 device was stationary mounted on a fixed location to continuously measure the incident/reflected irradiance above snow cover. This location was always snow-covered during the 12-day ice station period.

The spectral albedo ($\alpha[\lambda]$) of a particular wavelength (λ) is:

$$\alpha(\lambda) = F\uparrow(\lambda)\, F\downarrow(\lambda)^{-1} \quad (1)$$

where $F\uparrow(\lambda)$ and $F\downarrow(\lambda)$ are the reflected and incident irradiances, respectively.

Considering multiple strong atmospheric water absorption bands across the 950–2500 nm wavelengths, the integrated albedo is calculated at various wavelength ranges (350–950 nm, 350–1300 nm, 350–2200 nm, and 350–2500 nm) to examine the spectral integrated albedo on different wavelengths. The 350–950 nm wavelength is mostly free of water absorption bands, and comparable with the Schooner Tara drift (Nicolaus et al., 2010). The 350–1300 nm wavelength range accounts for most of the energy from solar radiation (visible and near infrared spectrum) with a few water absorption bands. The 350–2200 nm wavelength range accounts for most of the information in irradiance measurements, without much instrument failure, error, or noise.

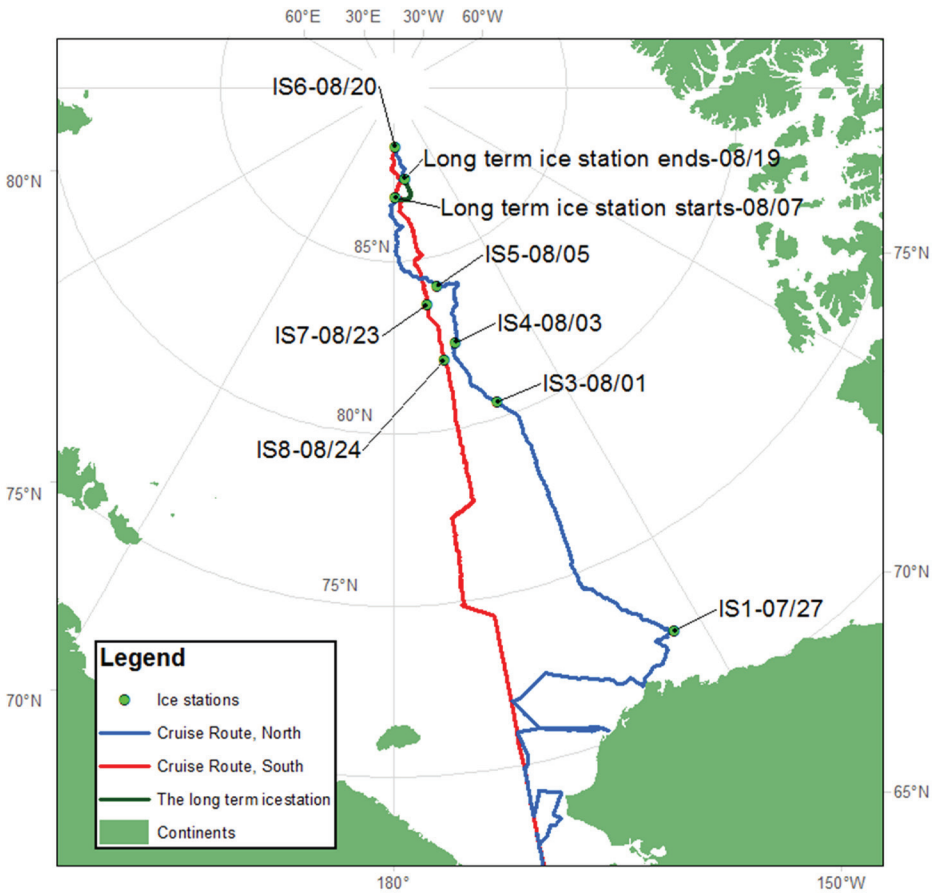

FIGURE 1. Location and date of short-term ice stations and long-term 12-day ice station during the 2010 Chinese National Arctic Research Expedition (CHINARE 2010) from July to August. (IS-1 and IS-3 to IS-8 mean short-term ice stations 1 and 3–8, with the date of the ice station attached as MM/DD. For the long-term ice station, the start/end date, location, and its drifting track are also marked on the map).

TABLE 1

Time and location of ice stations with radiometric measurements during the CHINARE 2010 (the start and end times are given by mm/dd and UTC time by 24 hours); coordinates are given by geographic lat/long, solar elevation is given by solar elevation angle; weather conditions are described by numbers (1 = no clouds, 2 = sunny day with scattered clouds, 3 = a cloudy day with the sun disc still visible, and 4 = an overcast day and the sun disc is totally obscured). There were no radiometric measurements in IS-2, and there were no albedo measurements in IS-6 and IS-8).

		Measurements start		Measurements end		Geographic coordinates		Solar	Weather
Ice Stations (IS)	Denoted as	Date	Time (UTC)	Date	Time (UTC)	Longitude	Latitude	elevation	condition
1st Short term IS	IS-1	07/27	01:00	07/27	05:00	152°34′W	72°18′N	33°	1–2
3rd Short term IS	IS-3	08/01	21:54	08/01	22:11	161°14′W	80°29′N	24°	4
4th Short term IS	IS-4	08/03	21:18	08/03	22:17	165°32′W	82°30′N	21°	1
5th Short term IS	IS-5	08/05	02:05	08/05	03:09	167°08′W	84°10′N	19°	3
12-day IS, 2nd day	L809	08/09	07:13	08/09	08:44	Continuous drifting, from 178°22′W, 86°48′N (L807) to 172°16′W, 87°20′N (L819)		12°–15°	1–4
12-day IS, 5th day	L811	08/11	21:51	08/11	22:29				
12-day IS, 6th day	L812	08/12	21:14	08/12	22:37				
12-day IS, 7th day	L813	08/13	21:10	08/14	03:28				
12-day IS, 10th day	L816	08/16	21:31	08/17	01:03				
12-day IS, 11th day	L817	08/17	21:00	08/18	04:20				
12-day IS, 12th day	L818	08/18	21:34	08/18	22:34				
6th Short term IS (no albedo)	IS-6	08/20	03:20	08/20	03:57	177°09′W	88°22′N	11°	2
7th Short term IS	IS-7	08/23	07:33	08/23	09:00	170°38′W	83°45′N	15°	3
8th Short term IS (no albedo)	IS-8	08/24	02:54	08/24	03:28	169°01′W	81°57′N	17°	1

The wavelength-integrated albedo (referred to as "integrated albedo" for short, $\alpha[\lambda_1,\lambda_2]$) at a wavelength range from λ_1 to λ_2 is calculated as:

$$\alpha\left(\lambda_1,\lambda_2\right)=\frac{\int_{\lambda_1}^{\lambda_2}F\uparrow\left(\lambda\right)}{\int_{\lambda_1}^{\lambda_2}F\downarrow\left(\lambda\right)},\ \lambda\in\left[\lambda_1,\lambda_2\right] \qquad (2)$$

where λ_1 = 350 nm, and λ_2 = 950, 1300, 2200, or 2500 nm, respectively. The selection of λ_2 is mainly affected by the distribution of water absorption bands.

FIELD MEASUREMENTS

The short-term ice stations (IS) were conducted along the cruise track, spanning across the marginal ice zone to the pack ice near the north pole, with various snow, bare ice, and melt pond surfaces observed during the one month period (Huang et al., 2013; Xie et al., 2013). The sea ice thickness was 1.2–3 m during the cruise (over 3 m on ridges), and the fresh snow depth ranged between ~5 and 15 cm (a few snowfall events occurred during the period [Xie et al., 2013]). The first short-term ice station (IS-1) was located at the marginal ice zone. The snow cover was all melted away, with a ~10-cm-thick loose granular ice (or bare ice) on the surface of sea ice (Xie et al., 2013). The IS-3, IS-4, and IS-5 were located in the pack ice zone, with a thin fresh snow cover (5–15 cm) on top of granular ice, and most of melt ponds were refrozen. During the 12-day ice station, most of the melt ponds observed were also refrozen. For this study, fresh snow over the refrozen melt pond is referred to as pond snow; the refrozen pond surface without fresh snow cover is referred to as pond ice. The IS-7 and IS-8 were conducted on the southward leg after the 12-day ice station. The sea ice in the last two ice stations was not covered by fresh snow, and melt pond was not covered by ice or snow. By visual inspection and calculation, the melt pond coverage ranged from 20% to 30% for all the short-term stations (Xie et al., 2013).

In each of the short-term ice stations, albedo measurements took 2–4 hours (Table 1). In the 12-day ice station, albedo measurements took around 2 hours per day. In each of the short-term ice stations, several sets of repeated measurements were conducted on different sea ice surfaces, such as bare ice and melt pond water in marginal ice zone, or snow cover and frozen melt ponds in the central Arctic Ocean. For each set of measurements, the incident solar irradiance was first measured, and then the reflected irradiance from the surface objects (within a few minutes). The measurements were conducted along one or two transects passing through snow/bare ice surfaces and melt ponds, to quantify the albedo change from snow/ice surface to melt pond and then snow/ice surface, with a fixed 100 cm interval between any two adjacent measurements. With the 1 m pole in hand, the sensor could be held above the center of a melt pond (given a pond was not too big). By walking along the melt pond, the sensor measured the reflected irradiance along a transect passing through the melt pond. The total incident solar irradiance (350–2500 nm) measured during the 2–4 hours of measurements does not differ greatly. Their standard deviations across the incident irradiation measured during the 2–4 hours of each day were only

TABLE 2

Incident and reflected energy fractions on different wavelength ranges compared to the total irradiance at 350–2500 nm wavelength range.

		Energy fractions by wavelength range		
Ice station	Object	350–950 nm	350–1300 nm	350–2200 nm
IS-1	Sky	0.7395	0.9260	0.9996
IS-5	Sky	0.7539	0.9416	0.9996
IS-7	Sky	0.7924	0.9463	0.9986
L809	Sky	0.7172	0.9331	0.9984
L811	Sky	0.8155	0.9659	0.9995
L813	Sky	0.8168	0.9584	0.9972
L816	Sky	0.8292	0.9841	0.9990
L817	Sky	0.7659	0.9473	0.9994
IS-1	Granular Ice	0.8902	0.9904	0.9996
IS-5	Snow	0.8483	0.9858	0.9992
L811	Snow	0.8916	0.9909	0.9990
L813	Snow	0.9025	0.9884	0.9955
L816	Snow	0.8837	0.9748	0.9990
L817	Granular Ice	0.8980	0.9931	0.9989
IS-7	Granular Ice	0.9382	0.9926	0.9968
IS-5	Melt pond ice	0.8534	0.9850	0.9990
L809	Melt pond snow	0.8427	0.9828	0.9972
L809	Melt pond ice	0.8160	0.9789	0.9968
L813	Melt pond snow	0.9036	0.9885	0.9957
L811	Melt pond ice	0.8921	0.9903	0.9991
L813	Melt pond snow	0.9036	0.9885	0.9957
L813	Melt pond ice	0.9046	0.9873	0.9942
L816	Melt pond snow	0.8745	0.9676	0.9988
IS-7	Melt pond ice	0.9358	0.9833	0.9936

Note: The spectroradiometer was working on reflectance mode on IS-3 and IS-4, so the irradiance value is not included in the table)

0.16%–1.79% compared to the minimum incident irradiance measured in the same day/period. So the changes of solar irradiance could be neglected during each melt pond transect observation.

The 12-day ice station (86°48′ to 87°20′N) was started on 8 August and ended on 19 August (Table 1). It was located near the North Pole, with melt ponds partially covered by refrozen ice and fresh snow. Surface melting was not seen during that period until a rainfall event occurred on 17 August (Lei et al., 2012) and caused a substantial surface melting. A series of albedo observations was made with the handheld ASD spectroradiometer around several adjacent melt ponds. Two of these melt ponds were repeatedly measured to examine the albedo evolution in each day. A continuous albedo observation was done by the fixed CMA6 albedometer in another location through the same 12-day ice station period.

Results

MEASURED ALBEDOS IN DIFFERENT WAVELENGTH RANGES

During the 2–4 hours (Table 1) of the field work in one day, the variation in solar irradiance is negligible. However, the calculated albedo is still sensitive to such changing incident irradiation, so abnormal values (outlier values) of incident irradiance and albedos are removed to minimize such error.

The distribution of irradiation energy on the spectrum is expressed with the fraction between the energy in a specified wavelength range (350–950 nm, 350–1300 nm, and 350–2200 nm) and the total energy measured by the ASD device (Table 2). It is calculated as the following:

$$f(\lambda_1,\lambda_2)=\frac{\int_{\lambda_1}^{\lambda_2}F(\lambda)}{\int_{350}^{2500}F},\ \lambda\in[\lambda_1,\lambda_2] \tag{3}$$

where $f(\lambda_1,\lambda_2)$ is the fraction of energy as presented in Table 2, and λ_1 to λ_2 is the wavelength range whose irradiance is compared with the total measured irradiance (350–2500 nm). This fraction is calculated for both the incident irradiance and reflected irradiance.

By the calculation, the fractions of the incident irradiance at the 350–950 nm, 350–1300 nm, and 350–2200 nm wavelength ranges are ~72%–83%, ~92%–98%, and ~100% of the total incident irradiance at the 350–2500 wavelength, respectively (Table 2). For the reflected irradiance, around 82%–94%, 97%–99%, ~99%–100% of the total energy are distributed within the 350–950 nm, 350–1300 nm, and 350–2200 nm wavelength ranges, respectively. Thus, irradiance within the 350–1300 nm wavelength range accounts for over 92% and 97% of the incident and reflected energy, respectively. As there are substantial errors and noises at the 2200–2500 nm wavelength due to the water absorption band, the 350–2200 nm wavelength range is used in most wavelength-integrated albedo calculations of this study.

As 98% of the incident and reflected energy is concentrated in the 350–2200 nm wavelength, the comparison of surface albedo measured between the ASD FieldSpec (350–2200 nm wavelength range used) and CMA6 device (300–2800 nm) is feasible. In theory, snow albedo measured by the CMA6 should be slightly lower than that measured by the ASD. But this is not always true because of the different working environment of the two devices.

Integrated albedos are calculated by different wavelength ranges (Table 3). Clearly, the integrated albedo is usually lower when a wider wavelength range is used, with the highest albedos in 350–950 nm range. Such difference, however, is very small between 350–2200 nm wavelength and 350–2500 nm wavelength. There are also some exceptions, as the integrated albedo across a longer wavelength range could be slightly higher than that of a shorter wavelength range. This is caused by extremely high reflected irradiance in some of the water absorption band and extremely low incident solar irradiance in the same water absorption band.

SPECTRAL ALBEDO OF SNOW COVER AND GRANULAR ICE (BARE ICE)

Snow cover is a high scattering surface, featuring a high spectral albedo in the visible spectrum (380–750 nm). Increase in snow grain size substantially reduces the surface albedo of snow, because an incident photon has to travel a longer distance in a larger grain, resulting in a higher probability that the photon is being absorbed before scattered (Warren, 1982). Increment of liquid water content in snow can also be considered as an increment in snow grain size, because snow grains and liquid water are optically similar in term of refraction (Warren, 1982). With the progression of summer surface melting, the snow grain melts and refreezes together—that is, increasing the snow grain size and liquid water content, therefore reducing the snow surface albedo. A rainfall event also leads to the increment of both grain size and liquid water content. In contrast, fresh snow from a snowfall event is relatively dry, having a smaller grain size, and a higher surface albedo than old, dense and wet snow.

The patterns of the spectral albedo of snow and granular ice varied across different ice stations and days (Fig. 2, parts a

TABLE 3

Mean integrated albedos in different wavelengths for each ice station or each day.

		Wavelength range (nm)			
Ice stations	Objects	350–950	350–1300	350–2200	350–2500
IS-1	Granular ice	0.7234	0.6805	0.6370	0.6370
IS-3	Snow	0.7434	0.6902	0.6553	0.6552
IS-4	Snow	0.7781	0.6379	0.5988	0.5990
IS-5	Snow	0.7812	0.7353	0.7283	0.7284
L809	Snow	0.8858	0.8103	0.7693	0.7698
L811	Snow	0.8533	0.7244	0.7308	0.7311
L813	Snow	0.7751	0.7216	0.6975	0.6990
L816	Snow	0.7254	0.6740	0.6803	0.6804
L817	Snow	0.6235	0.5581	0.5319	0.5322
IS-7	Granular ice	0.7107	0.6336	0.6044	0.6037
IS-3	Melt pond ice	0.3927	0.3627	0.3465	0.3464
IS-4	Melt pond ice	0.4853	0.4368	0.4111	0.4113
IS-5	Melt pond ice	0.6431	0.5980	0.5980	0.5980
L809	Melt pond ice	0.7437	0.6813	0.6485	0.6496
L809	Melt pond snow	0.8044	0.7213	0.6839	0.6844
L811	Melt pond ice	0.7245	0.6790	0.6621	0.6623
L811	Melt pond snow	0.7193	0.6782	0.6615	0.6618
L813	Melt pond ice	0.5853	0.5449	0.5277	0.5290
L813	Melt pond snow	0.6454	0.6007	0.5805	0.5812
L816	Melt pond snow	0.5840	0.5441	0.5532	0.5533

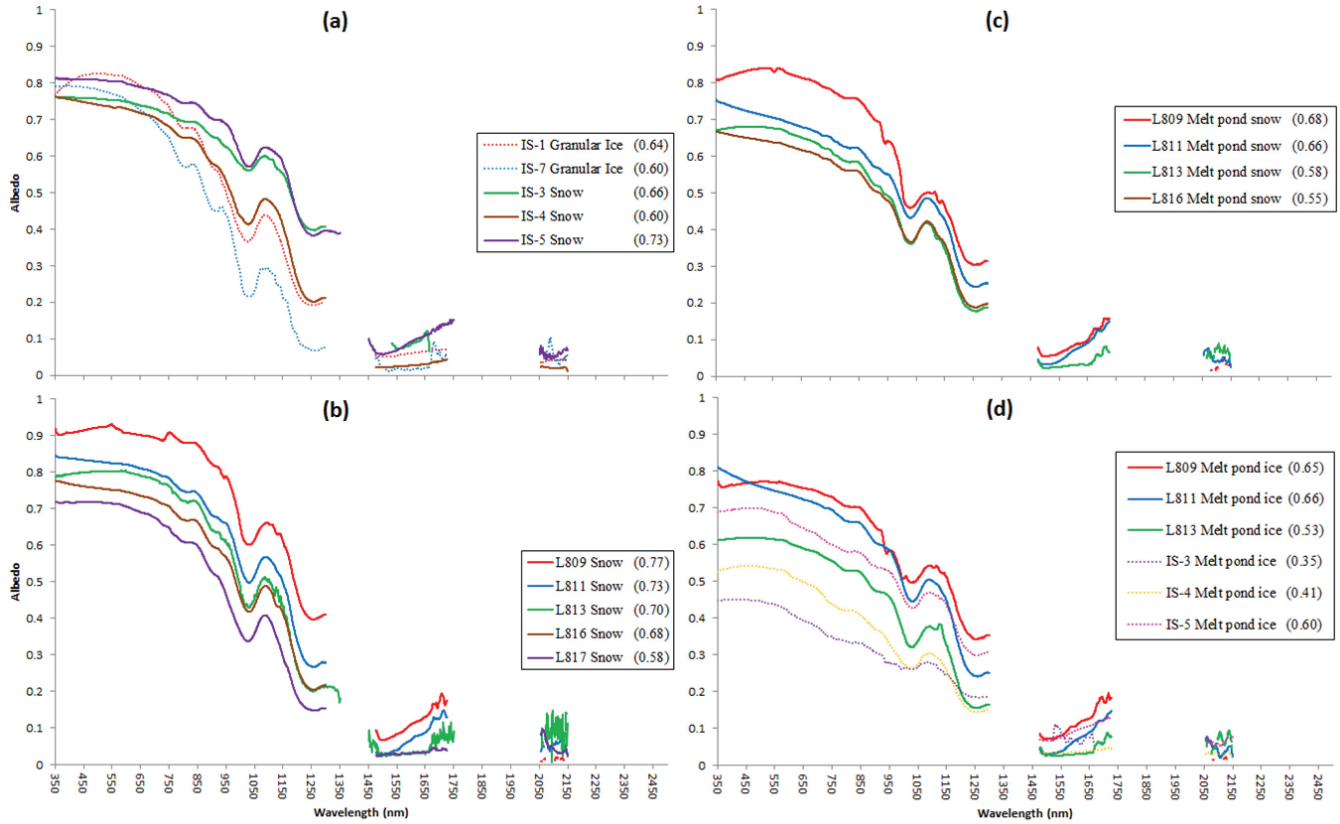

FIGURE 2. Mean spectral albedo (wavelengths that are affected by strong water absorption are not plotted). (a) Granular ice (or bare ice) and snow albedo at short-term ice stations, (b) Snow albedo at 12-day ice station, (c) melt pond snow albedo at 12-day ice station, and (d) melt pond ice albedo. (IS-1, IS-3, IS-4, IS-5, and IS-7 stand for short-term ice stations 1, 3, 4, 5, and 7; L809, L811, L813, L816, L817 stands for 9, 11, 13, 16, and 17 August 2010, during the 12-day ice station. Values in brackets denote the integrated albedo at 350–2200 nm wavelength range).

and b). The surface albedo of granular ice (around 0.56–0.68) did not differ greatly from snow albedo measured on the short-term ice station 3 and 4 (~0.59–0.69 for IS-3, ~0.49–0.76 for IS-4). When latitude of the ice station became higher, snow albedo (~0.61–0.8) became higher than the granular ice albedo, except when the snow became wet (~0.50–0.61 of L817) after a rainfall event, since wet snow or granular ice absorbs more near-infrared irradiation (Lei et al., 2012). (Note the data ranges specified here are the 5th and 95th percentile of all data measured of the same surface object, not the minimum or maximum value of the mean albedo [which are listed in Table 3] of the specified surface object of each day). Snow albedo measured in the short-term ice stations IS-3 and IS-5 shows similar albedo-wavelength patterns, with higher values in IS-5. This difference was due to a snowfall event in the IS-5, resulting in a fresh snow over the old snow or bare ice. The snow albedos measured in IS-4 have a much lower albedo in infrared band. This represents a relatively older and denser snow cover with relatively aged, coarse grains and an average thickness of 10 cm (Wiscombe and Warren, 1980).

The snow albedo measured during the 12-day ice station was continuously declining (Fig. 2, part b). Fresh snow observed in L809 had a very high visible band albedo (>0.90) around 550 nm, which contributed most to the high integrated (350–2200 nm) albedo around 0.77. The albedo-wavelength curves of L813 and L816 have a similar pattern as that of L809, but it is lower across all wavelengths measured. The lowest snow albedo occurred in the L817, since a rainfall event in this day caused significant snow melting.

MELT POND SPECTRAL ALBEDO CHANGES

Compared with snow and ice, the refrozen melt pond spectral albedos are relatively lower in visible bands (Fig. 2, parts c and d). Most of the integrated albedo of refrozen ice on melt pond (0.32–0.67) is lower than the snow over ice on melt pond (0.49–0.71).

The refrozen ice over pond in the ice station 3 (IS-3) was very thin (<2 cm) with lower albedo (0.35), as solar radiation transmitted through the thin ice was absorbed by underlying water. The ice over melt pond of IS-5 was thicker with even some fresh snow patches on ice, so the spectral albedo was higher in all wavelengths, resulting in a much higher integrated albedo (0.60).

Most of the melt ponds in the 12-day ice station had a frozen surface with snow patches on top. The spectral albedo pattern of pond snow is similar to that of snow outside the pond, although the spectral albedo measured is lower in nearly all wavelengths (comparing b and c). Refrozen pond ice shows a lower albedo in visible bands and a relatively higher albedo in the near infrared bands, as compared with the melt pond snow (comparing c and d). After the higher pond ice albedo measured in L809 and L811 (~0.65–0.66), it decreased to ~0.53 (L813). Melt pond with water showed a large albedo variation ranging from 0.16 (deep water) to 0.44 (patchy water layer above a refrozen ice surface).

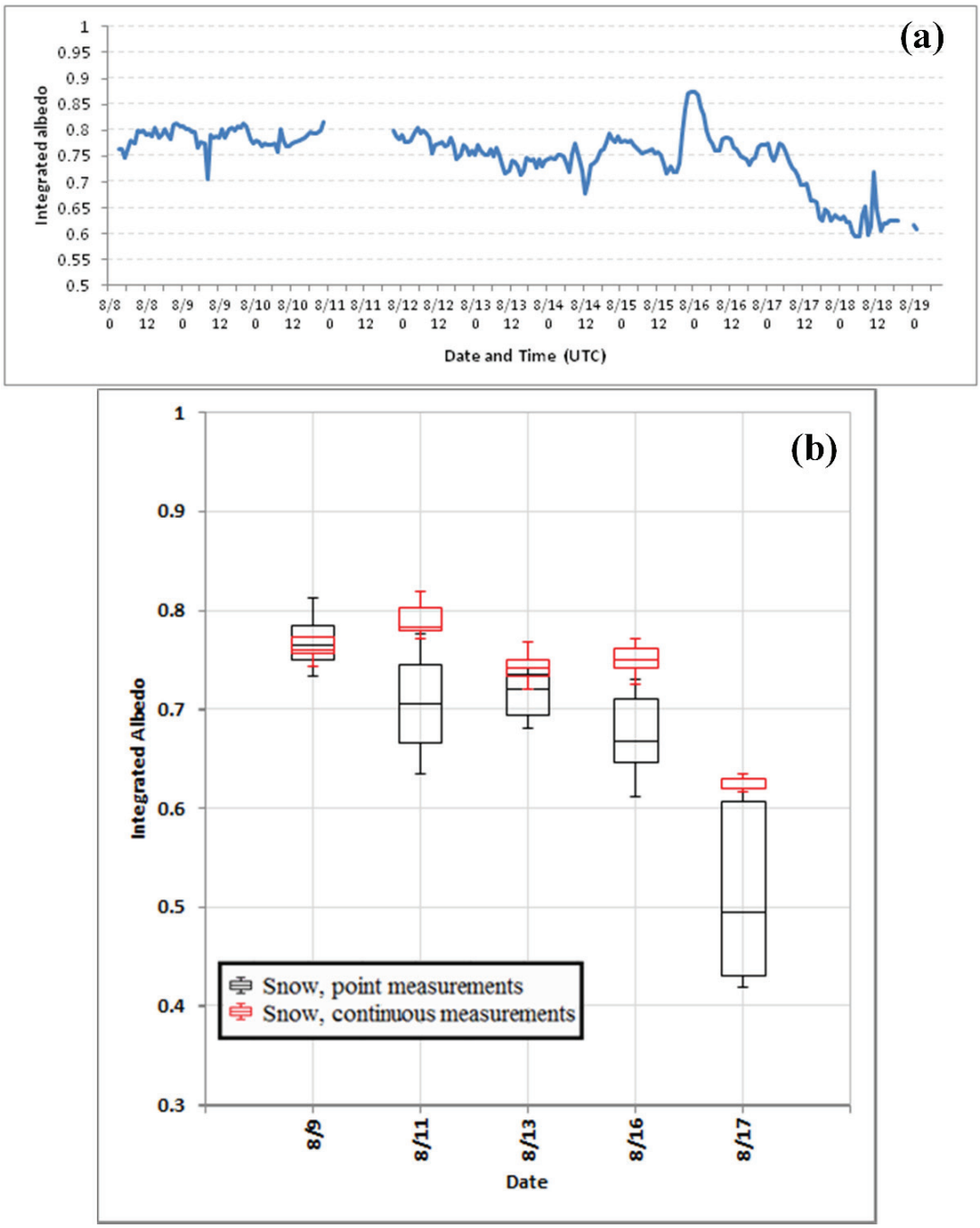

FIGURE 3. (a) Hourly albedo of snow covered sea ice measured by the fixed CMA6 device during the long-term ice station; and (b) concurrent albedo comparison of CMA6 and ASD Field Spec on snow covered sea ice, but in different locations. Dates are given as M/DD.

TEMPORAL AND SPATIAL ALBEDO CHANGES

The continuous measurements by the fixed CMA6 device over snow-covered sea ice conducted during the period of 12-day ice station are shown in Figure 3, part a. Although the instrument had data losses due to several instrument issues, it provides the mostly consistent time series of snow albedo during the time period. Taking a closer look at the albedo time series (Fig. 3, part a), two obviously different periods separated at 6:00 UTC 17 August (or 18:00 16 August local time), when a rainfall event occurred, which resulted in snow melt and albedo drop. Before this time, although there was some variation from hour to hour and from day to day, integrated albedo measured were mostly around 0.75–0.8, with one abnormally high albedo 0.87 during the 21:30 UTC (15 August) to 1:30 UTC (16 August) (or 9:30–13:30, 15 Aug, in local time). The primary reason of this high albedo was due to a new snowfall event that occurred when the temperature dropped

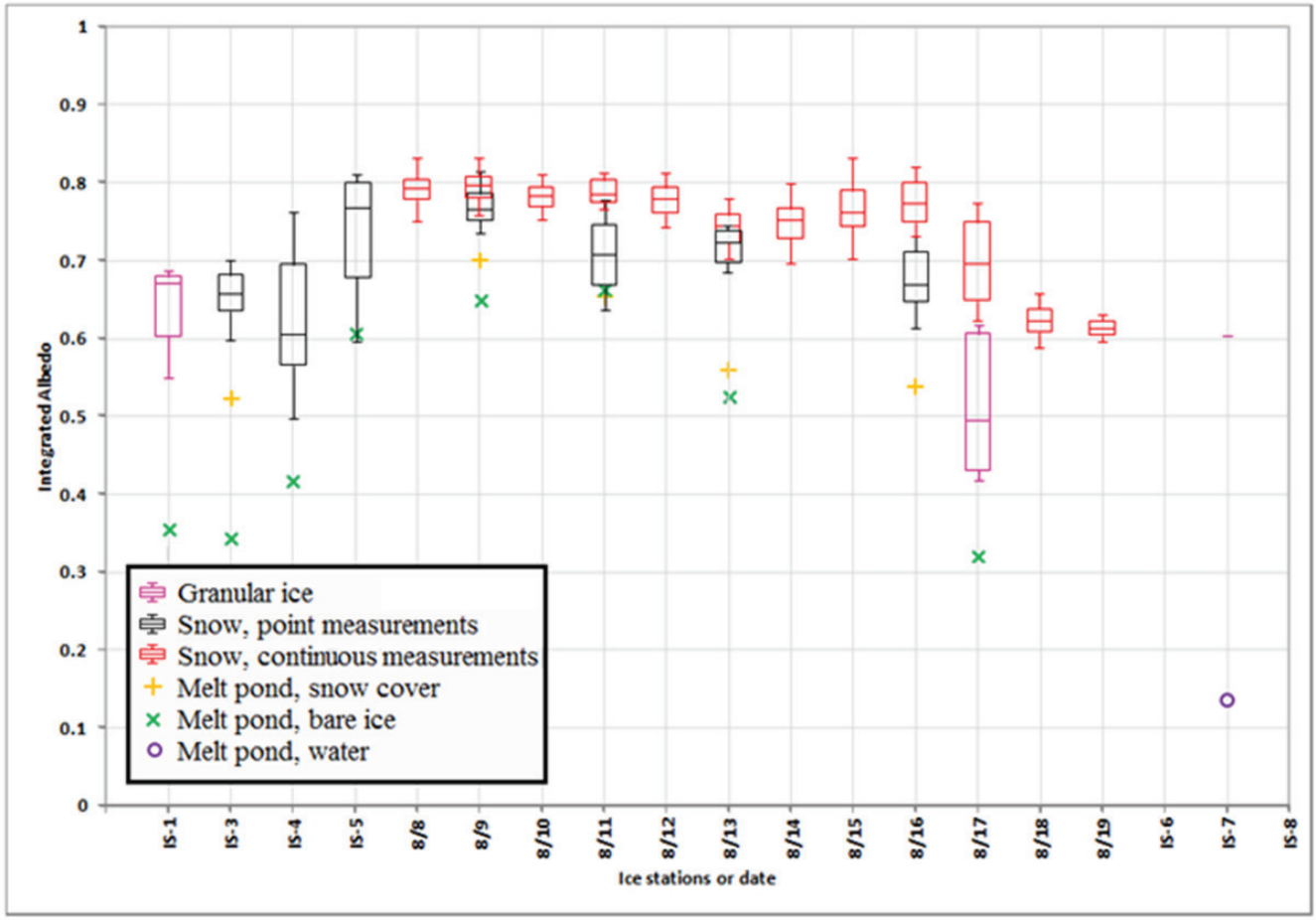

FIGURE 4. Integrated albedo (350–2200 nm wavelength) of point and continuous measurements in all ice stations (The boxes indicate the first, second (median), and third quartile, and the upper and lower whisks indicate the 5th and 95th percentile).

to –4 °C in this period (Fig. 3 of Xie et al., 2013). As the CMA6 device was properly heated and ventilated, the higher albedo could also be caused by snow on the upward-looking sensor, which lowered the measured incident flux. About 27 hours later, the temperature rose to 2 °C, and a rainfall event (17 August) occurred and caused extensive snow melt and a large albedo drop thereafter, to ~0.6 during 18 and 19 August. The impact of this weather event is also seen with the ASD observed surface albedo during the same period, with the much lower snow and melt pond albedo observed on 17 August (Fig. 3, part b).

Weather events could be one of the decisive factors that determine the local, short-term rapid change of surface albedo. However, for albedo variation on a larger scale, the temporal and spatial variation should also be addressed.

Figure 4 puts all albedo measurements of the entire cruise into one plot so an overall picture of albedo evolution may be drawn. Generally, when the cruise was going north from the IS-1 (72°18′N), IS-3 (80°29′N), IS-4 (82°30′N), IS-5 (84°10′N), and L809 (87°N), surface albedos were all increasing. Higher surface albedo in the IS-5 and L809 can be partially attributed to the snowfall events. The daily median albedo of snow in the 12-day ice station from 8 to 19 August shows a similar pattern as the hourly mean albedo (Fig. 3), in two stages. Before 17 August, the snow albedos mostly ranged between ~0.75 and 0.8; after the rainfall event 17 August, the snow albedo rapidly decreased to ~0.6. Refrozen melt pond albedos increased from IS-1 to 9 August, and then rapidly decreased from 9 to 17 August.

The 12-day ice station is an excellent opportunity to compare the point measurements and continuous measurements of snow albedo in the same floe but different locations. During the 12-day ice station, pond snow albedo was steadily decreasing from 0.68 to 0.55 (L809 to L816), as described in section 3.4. It is seen that the point measurements of snow albedo were usually lower than the daily median snow albedo of continuous measurements. Overall, however, the point measurements showed higher variation (standard deviation of 0.03 to ~0.11 in terms of albedo, within one day) than the continuous measurements (standard deviation of 0.006 to ~0.017 in terms of albedo, within one day). This was most likely due to mixed signals of different surface types and different locations during the point measurements, while the continuous measurements were entirely automated and fixed at the same location.

ALBEDO CHANGES THROUGH THE HETEROGENEOUS MELT POND TRANSECTS

During the 12-day ice station, it was possible to examine the albedo evolution/change and variation along the same pond transect through repeated measurements. The mean ice thickness of the floe used for the 12-day ice station was ~2 m, with pond depth of 20–40 cm. The refrozen ice on pond surface was usually less than 2 cm in thickness. For example, one melt pond was measured on 9 August (L809), 13 August (L813), and 16 August (L816) (Fig.

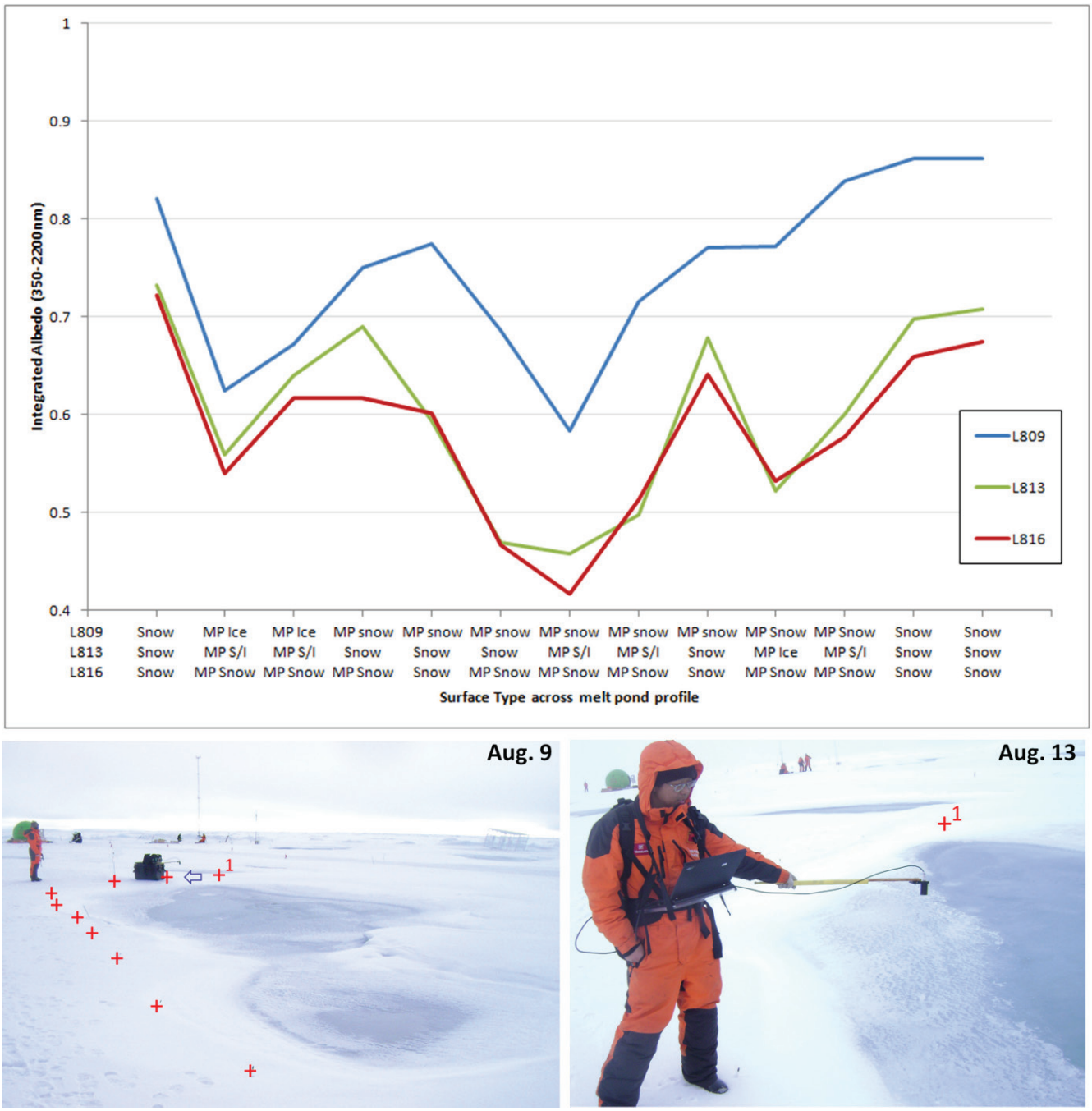

FIGURE 5. Repeated measurements of albedo transects (top) passing through the same melt pond (bottom). The interval between red crosses is 100 cm. the first location on snow is marked in both photos, with last two locations also on snow (MP S/I means a mixture of melt pond snow and ice; water means melt pond water).

5). In L809, new snow covered a large portion of the pond surface, so the albedo at the pond center was around 0.58 and the albedo of melt pond snow was higher, ranging from 0.7 to 0.8, and even higher than 0.8 on snow surfaces outside of the pond. In L813, the thinned pond ice had a reducing albedo as low as 0.46. Later in the L816, surface albedo across the profile dropped again, to around 0.61 for snow-covered melt pond ice, and 0.41 for extremely thin ice in the center, partially due to snow packing and surface melt over the frozen pond. The snow cover was very patchy over the pond, while the thinning pond ice was a decisive factor for the surface albedo of the same pond.

Discussions

MEASUREMENT ERRORS

There could be several sources of error associated with the field measurement method when calculating the spectral and in-

tegrated albedo. First, as the solar irradiance was measured before the downward-looking measurements, changes of solar disc condition associated with cloud and fog conditions would cause noticeable changes in the incident solar radiation of the visible bands. This error is minimized by excluding abnormal data values as done in this study.

The second source would be the inherent instrument noise, which cannot be ignored when the measured irradiance was extremely low. Such errors were substantial on the 1300–2500 nm wavelength, with low irradiance caused by multiple high water absorption bands within these wavelengths. Such error severely affects the calculation of spectral albedo, which led to abnormally high spectral albedo on water absorption bands. So, wavelengths with high water absorption are not considered in the analysis of surface spectral albedo changes.

The third source is the reflected energy from nearby snow or ice when measuring a melt pond. As the cosine sensor collects reflected energy from an entire hemisphere, it could be difficult to define a fixed sensor footprint size. For the context of this field work, when the handheld pole was 1 m long and the sensor was positioned 1 m above the surface, over 80% of the reflected irradiance came from a 1-m radius circle around the nadir point (personal communication with Don Perovich). So the measured irradiance was actually a mixed signal, with a small portion (<20%) of reflected irradiance originating from adjacent snow cover or granular ice outside the ponded water or ice. Generally, albedo measured on a pond center should be the lowest. On a large melt pond transect, the situation is much more complicated, as the melt pond surface itself was a heterogeneous surface of refrozen melt pond and snow patches. These, of course, will be mixed pixels viewed from a satellite pixel field of view. Therefore, a mixed albedo from field measurements might be a better reality if compared with satellite data.

VARIATIONS IN MEASURED SURFACE ALBEDO

Similar surface objects can have highly varied albedo in a rapidly changing Arctic summer. On the 350–2200 nm wavelengths, the albedo spectra of surface snow and granular ice outside of melt ponds tend to have similar patterns, but their integrated albedo varies, from 0.60 of granular ice (IS-7), to 0.77 of new snow surface (L809). It should also be noted that, as the IS-7 was located in a high-latitude area (around 80°N), its granular ice albedo (0.60) was lower than that (0.64) measured in the marginal ice zone (IS-1). Such rapid reduction, change, or variation could also be seen during the last days of the 12-day ice station. The snow albedo reduced from around 0.75–0.8 (before 17 August) to 0.6 (after 17 August). Melt pond surface albedo is determined by water, water depth, ice thickness (and snow if appears over ice), and inherent optical properties of ponded ice (which is different on the pond of first-year or multi-year ice). The albedo of these melt ponds shows an evident temporal decreasing trend (seen in the 12-day ice station), and an increasing trend with the increase of latitude.

The spectral albedo also varied for different surface objects. In the same day, the visible band spectral albedo difference between snow and melt pond ice is the most obvious at ~550 nm wavelength (the snow albedo around this wavelength is ~0.1–0.2 higher than that of melt pond snow/ice albedo). For the infrared band, such differences were most obvious at ~1025 nm (the snow albedo around this wavelength is around 0.05–0.175 higher than that of melt pond snow/ice albedo), but much less obvious from 1025–1300 nm wavelength (the snow albedo in this wavelength range is no more than 0.05 higher than that of the melt pond snow/ice albedo). For snow and ice surface, change in total reflected energy is substantially affected by surface structure evolution, because reflected energy in visible band accounted for most of the total reflected energy, and visible band surface reflectance is then determined by surface structure. As the surface structure is highly sensitive to events like snowfall (a new, high-scatter snow cover on sea ice and melt pond) or rainfall (causing rapid surface melting and wet snow/ice), resulting rapid surface albedo changes in hours.

COMPARISON WITH OTHER FIELD OBSERVATIONS

According to the 1997–1998 SHEBA ice station measurements (Perovich et al., 2002) on the multiyear sea ice from around 75°N,142°W to 80°N, 162°W (in the Arctic ice cap far north of Alaska), the spring surface albedo of multiyear sea ice (snow covered) was ~0.8–0.9. This was measured on a dry and homogeneous snow-covered ice surface. With the onset of summer melting near the end of May 1998, the surface albedo decreased to ~0.7. Later during June 1998, the albedo of the refrozen melt ponds was ~0.5–0.7, and decreased to 0.4 when the melt ponds were covered with water only during July and August (Table 4).

Albedo measurements collected by Perovich et al. (2002) in SHEBA were integrated at 300–3000 nm with multiple devices. With the energy fractions as shown in Table 2, their results in summer could be compared with the ASD-measured surface albedo during the 12-day ice station of CHINARE 2010 (located around 87°N). The integrated albedo calculated in the SHEBA utilized a wider wavelength range, which should lead to a slightly lower integrated albedo than that of CHINARE 2010, but such difference could be negligible compared to the spatial and temporal differences. Generally, snow albedo measured during 10 to 16 August of the 12-day ice station of CHINARE 2010 is slightly lower than that of the SHEBA in summer, and the refrozen pond albedo is similar (Table 4).

The Schooner Tara transpolar drift (Nicolaus et al., 2010) observed Arctic multiyear sea ice albedo and transmittance with a high temporal resolution. Most of the albedo observations were conducted during the drift around 86°N to 89°N in the Atlantic sector of the Arctic, with an integrated albedo calculated at 350–950 nm. The Tara observations continuously measured mean surface albedo by a set of fixed spectroradiometers. Compared to the SHEBA observations, the stages of melt pond development in the Tara observation were similar, but the measured albedo was much higher, due to different latitude of the field observations, and narrower wavelength range. Compared to the 12-day ice station of this study, the measured surface albedo can be compared with the ASD measured albedo integrated at the 350–950 nm wavelength range, observed during 10–16 August of the 12-day ice station (Table 4). Only the surface albedo measured on 17 August of CHINARE 2010 was considerably lower than the mean surface albedo measured during the 86°N to 89°N of the Tara observation, because of the rainfall event triggered surface melting.

The surface observations were conducted on seasonal fast ice by Barrow, Alaska, field experiment (Perovich and Polashenski, 2012) during 2000, 2001, 2008, and 2009. This field experiment addressed the differences between seasonal and multiyear sea-ice albedo evolution. In addition, the variation of seasonal sea-ice albedo evolution in different years was also discussed (Perovich and Polashenski, 2012). The integrated albedos of these measurements were calculated at 300–3000 nm wavelength range, which should be comparable to the integrated albedo at 350–2200 nm wavelength range as we did here. Like the SHEBA observation, integrated albedo calculated from this Barrow, Alaska, observation should be slightly lower. The melting process in Barrow, Alaska, occurred ear-

TABLE 4

Comparison of different arctic surface albedo observations in melting months.

		Surface Albedo		
Field experiments	Wavelength range (nm)	Wet snow	Ponds refrozen	Ponds water
SHEBA 1998	300–3000	~0.70–0.80	~0.50–0.70	~0.40–0.50
CHINARE 2010[1] (this study)	350–2200	~0.68–0.76	~0.52–0.68	~0.32–0.41
Barrow Alaska[2]	300–3000	~0.6	~0.54	~0.2
TARA 2007	350–950	~0.72–0.84	~0.66 minimum[3]	
CHINARE 2010 (this study)	350–950	~0.72–0.85	~0.58–0.72	~0.38–0.43

[1]Wavelength range of the instrument is 350–2500 nm, but the wavelength-integrated albedo is calculated at 350–2200 nm wavelength range because of substantial error at the water absorption band at 2200–2500 nm.

[2]The Barrow Alaska field experiments were conducted in the summer of 2000, 2001, 2008, and 2009.

[3]Albedo observation of the Schooner Tara drift was done by fixed instruments; thus, there is no dedicated melt pond observation available.

lier than the CHINARE site. The albedo observation during Junes of the four years of the field experiment in Barrow, Alaska, is comparable with the result of CHINARE site during August (Table 4). During the Augusts of Barrow, Alaska, experiment, a much lower surface albedo (0.2) was observed, because the bottom ice of melt pond was all melted away and only melt pond water was measured. This is comparable to the melt pond observation of the IS-1 (located on marginal ice zone) and the IS-7 (conducted in the end of August) of CHINARE 2010, with melt pond water albedo of ~0.20. During August and September, only sea water with nearly zero albedo can be observed at the field experiment site in Barrow, Alaska.

Summary and Conclusion

Surface albedo measurements were conducted during the CHINARE 2010 on various sea ice surface objects on seven short-term and one 12-day ice stations. These observations were done across the rapidly changing marginal ice zone into the pack ice zone in the center of the Arctic Ocean, from seasonal ice in lower latitudes to multi-year ice near the North Pole. The granular ice and melt pond water were observed in the marginal ice zone, and at the end of the cruise. When the ice breaker reached higher latitudes, several snowfall events occurred, leading to a rapidly increasing albedo. During the 12-day ice station, the albedo of refrozen melt ponds was reducing, because the thinner ice of the pond surface and the patchy snow cover over the thinner ice was aging. Later, due to the 17 August rainfall event, the melting process of refrozen melt pond was accelerated and water was even observed on thin ice of the pond. In the meantime, the snow cover became wet and melted away, and the refrozen ice surface of pond became much thinner, leading to a rapid decreasing in surface albedo of the pond.

The albedo change of snow-covered ice during the 12-day ice station was mostly affected by weather events. On a local scale, a snowfall event can greatly increase the surface albedo, thus dampening the ice-albedo feedback, while a rainfall event has the opposite effect. The surface albedo change observed in the CHINARE 2010 was highly varied temporally and spatially, and the albedo evolution and ice-albedo feedback were heterogeneously distributed.

The surface albedo differences between snow-covered ice and melt pond were evident and highly variable. The integrated snow surface albedo was ~0.15 higher than the frozen melt pond albedo in 9 August, while such difference was 0.40 after the 17 August (granular ice compared with melt pond water). As the 12-day ice station was conducted on a over 100 km2 ice floe with around 30% melt pond coverage (Xie et al., 2013), the surface albedo changes of melt pond was one of the determining factors in the sea ice surface albedo changes. In addition, across different ice stations of the cruise, the snow grain aging and melt pond development were highly varied, causing an albedo difference of more than 0.1 for the same type of surface object in different times and/or locations. Thus, the development stages of melt pond are very important for the parameterization of regional albedo in climate models (Liu et al., 2007). These parameters and thresholds should be considered according to different times and areas, to accommodate these heterogenetic and rapid changes.

Acknowledgments

This work was partially supported by the Chinese Polar Environment Comprehensive Investigation & Assessment Programs (No. CHINARE2015-04-03), the Foreign Cooperation of Chinese Arctic and Antarctic Administration (No. IC201301), and the National Nature Science Foundation of China (No. 41371391). Travel expenses for Xie to the cruise were covered by the National Oceanic and Atmospheric Administration's (NOAA's) Climate Research/Sea Ice Outlook Program. We sincerely acknowledge the support from the Chinese Arctic and Antarctic Administration, the Chinese Arctic Expedition Team-2010, and the other persons of the sea ice team of the cruise. Thank you to Don Perovich for providing the cosine sensor for field work.

References Cited

Barry, R. G., 1996: The parameterization of surface albedo for sea ice and its snow cover. *Progress in Physical Geography*, 20(1): 63–79, http://dx.doi.org/0.1177/030913339602000104.

Bitz, C. M., Holland, M. M., Weaver, A. J., and Eby, M., 2001: Simulating the ice-thickness distribution in a coupled climate model. *Journal of Geophysical Research*, 106(C2): 2441–2463, http://dx.doi.org/10.1029/1999JC000113.

Curry, J. A., Schramm, J. L., and Ebert, E. E., 1995: Sea ice-albedo climate feedback mechanism. *Journal of Climate*, 8(2): 240–247, http://dx.doi.org/10.1175/1520-0442(1995)008<0240:SIACFM>2.0.CO;2.

Ebert, E. E., and Curry, J. A., 1993: An intermediate one-dimensional thermodynamic sea ice model for investigating ice-atmosphere interaction. *Journal of Geophysical Research*, 98(C6): 10085–10109, http://dx.doi.org/10.1029/93JC00656.

Gardner, A. S., and Sharp, M. J., 2010: A review of snow and ice albedo and the development of a new physically based broadband albedo parameterization. *Journal of Geophysical Research*, 115: F01009, http://dx.doi.org/10.1029/2009JF001444.

Grenfell, T. C., and Perovich, D. K., 2004: Seasonal and spatial evolution of albedo in a snow-ice-land-ocean environment. *Journal of Geophysical Research*, 109: C01001, http://dx.doi.org/10.1029/2003JC001866.

Hanesiak, J. M., Barber, D. G., De Abreu, R. A., and Yackel, J. J., 2001: Local and regional albedo observations of Arctic first-year sea ice during melt ponding. *Journal of Geophysical Research*, 106(C1): 1005–1016, http://dx.doi.org/10.1029/1999JC000068.

Holland, M. M., Bitz, C. M., and Tremblay, B., 2006: Future abrupt reductions in the summer Arctic sea ice. *Geophysical Research Letters*, 33(23): L23503, http://dx.doi.org/10.1029/2006GL028024.

Huang, W., Lei, R., Ilkka, M., Li, Q., Wang, Y., and Li, Z., 2013: The physical structures of snow and sea ice in the Arctic section of 150°–180°W during the summer of 2010. *Acta Oceanologica Sinica*, 32(5): 57–67, http://dx.doi.org/10.1007/s13131-013-0314-4.

Lei, R., Zhang, Z., Ilkka, M., Cheng, B., Li, Q., and Huang, W., 2012: Reflection and transmission of irradiance by snow and sea ice in the central Arctic Ocean in summer 2010. *Polar Research*, 31: 17325, http://dx.doi.org/10.3402/polar.v31i0.17325.

Liu, J. P., Zhang, Z. H., Inoue, J., and Horton, R, M., 2007: Evaluation of snow/ice albedo parameterizations and their impacts on sea ice simulations. *International Journal of Climatology*, 27(1): 81–91, http://dx.doi.org/10.1002/joc.1373.

Lindsay, R. W., and Rothrock, D. A., 1994: Arctic sea ice albedo from AVHRR. *Journal of Climate*, 7(11): 1737–1749, http://dx.doi.org/10.1175/1520-0442(1994)007<1737:ASIAFA>2.0.CO;2.

Morassutti, M. P., and Ledrew. E. F., 1996: Albedo and depth of melt ponds on sea ice. *International Journal of Climatology*, 16: 817–838, http://dx.doi.org/10.1002/(SICI)1097-0088(199607)16:7<817::AID-JOC44>3.0.CO;2-5.

Moritz, R. E., and Perovich, D. K., 1996: Surface heat budget of the Arctic Ocean science plan. *ARCSS/OAII Rep*, 5: 64.

Nicolaus, M., Gerland, S., Hudson, S. R., Hanson, S., Haapala, J., and Perovich, D. K., 2010: Seasonality of spectral albedo and transmittance as observed in the Arctic Transpolar Drift in 2007. *Journal of Geophysical Research*, 115: C11011, http://dx.doi.org/10.1029/2009JC006074.

Pedersen, C. A., and Winther, J., 2005: Intercomparison and validation of snow albedo parameterization schemes in climate models. *Climate Dynamics*, 25(4): 351–362, http://dx.doi.org/10.1007/s00382-005-0037-0.

Perovich, D. K., and Polashenski, C., 2012: Albedo evolution of seasonal Arctic sea ice. *Geophysical Research Letters*, 39: L08501, http://dx.doi.org/10.1029/2012GL051432.

Perovich, D. K., Grenfell, T. C., Light, B., and Hobbs, P. V., 2002: Seasonal evolution of the albedo of multiyear Arctic sea ice. *Journal of Geophysical Research*, 107(C10): 8044, http://dx.doi.org/10.1029/2000JC000438.

Perovich, D. K., Richter-Menge, J. A., Jone, F., Light, B., Elder, B. C., Polashenski, C., Laroche, D., Markus, T., and Lindsay, R., 2011: Arctic sea-ice melt in 2008 and the role of solar heating. *Annual of Glaciology*, 52(57): 355–359.

Robinson, D. A., Serreze, M., Barry, R. G., Scharfen, G., and Kukla, G., 1992: Large-scale patterns and variability of snowmelt and parameterized surface albedo in the Arctic Basin. *Journal of Climate*, 5(10): 1109–1119, http://dx.doi.org/10.1175/1520-0442(1992)0052.0.CO;2.

Stroeve, J. C., Maslanik, J., Serreze, M. C., Rigor, I., Meier, W., and Fowler, C., 2011: Sea ice response to an extreme negative phase of the Arctic Oscillation during winter 2009/2010. *Geophysical Research Letters*, 38(2): L02502, http://dx.doi.org/10.1029/2010GL045662.

Warren, S. G., 1982: Optical properties of snow. *Review of Geophysics*, 20(1): 67–89, http://dx.doi.org/10.1029/RG020i001p00067.

Wiscombe, W. J., and Warren, S. G., 1980: A model for the spectral albedo of snow, I: Pure Snow. *Journal of the Atmospheric Sciences*, 37(12): 2712–2733, http://dx.doi.org/10.1175/1520-0469(1980)037<2712:AMFTSA>2.0.CO;2.

Xie, H., Lei, R., Ke, C., Wang, H., Li, Z., Zhao, J., and Ackley, S. F., 2013: Summer sea ice characteristics and morphology in the Pacific Arctic sector as observed during the CHINARE 2010 cruise. *The Cryosphere*, 7: 1057–1072, http://dx.doi.org/10.5194/tc-7-1057-2013.

Manuscript accepted May 2015